

# On the magnetic field architecture required to capture superparamagnetic nanoparticles in a microcapillary flow

Nicholas J. Darton · Bart Hallmark · Pulkit Agrawal · Tom James · Vincent H. B. Ho · Nigel K. H. Slater

Received: 12 December 2008 / Accepted: 1 March 2009 / Published online: 15 March 2009  
© Springer Science+Business Media B.V. 2009

**Abstract** The magnetic field required for the capture of superparamagnetic nanoparticles flowing in a microcapillary array under a constant pressure regime was investigated *in vitro*. It was found that the nanoparticles were captured in locations that varied significantly in magnetic field strength, and that the location of capture was strongly related to the net volumetric flow through the microcapillary array. A hypothesis is presented to explain these data in which the magnetic field of the trapping Neodymium Iron Boron (NdFeB) block magnet is divided into two zones that act differently on the nanoparticles. In the first ‘steering zone’, nanoparticles are moved closer to the capillary wall where they can be captured downstream in the second ‘capture zone’. This hypothesis can be used in the future to design magnetic field shapes for more effective particle capture at higher flow rates with lower field strengths.

**Keywords** Superparamagnetic nanoparticles · Microcapillary flow · In-flow capture · Magnetic field optimisation · Nanobiotechnology · Nanomedicine

## Introduction

The magnetic targeting of chemotherapeutic-bearing superparamagnetic nanoparticles to tumours offers an exciting route to reduce the side effects of chemotherapy. In addition, if these particles were to embolise the blood supply to the tumours (Sako et al. 1986), this would offer a two pronged attack on the cancerous tissue. To date, there have been three successful clinical trials of magnetic-targeted therapy of tumours in human patients (Lubbe et al. 1996, 1999; Wilson et al. 2004). In two of these trials, the chemotherapeutic drug epirubicin linked to 100 nm paramagnetic nanoparticles was administered intravenously. These nanoparticles were successfully targeted with minimal side effects to tumours with an externally applied 0.2–0.8 T magnet placed by the tumour (Lubbe et al. 1996, 1999). Wilson et al. (2004) delivered a sample of intra-arterially administered doxorubicin linked 0.5–5 µm superparamagnetic nanoparticles to tumours in patients with an external 1.5 T magnet placed adjacent to the tumour.

In order to further improve magnetic-directed therapeutic delivery, a better understanding of the dynamics of nanoparticle capture from physiological blood flow is required. To this end, several *in vitro* models have been constructed to explore the conditions for nanoparticle capture from flows (Sheng et al. 1999; Liu et al. 2001; Udrea et al. 2006; Kikura et al. 2007; Darton et al. 2008a, b; Le Drogoff et al. 2008; Darton et al. 2009). In these previous *in vitro*

N. J. Darton (✉) · B. Hallmark · P. Agrawal · T. James · V. H. B. Ho · N. K. H. Slater  
Department of Chemical Engineering and Biotechnology,  
New Museums Site, Pembroke St,  
Cambridge CB2 3RA, UK  
e-mail: njd28@cam.ac.uk

studies, it has been demonstrated that magnetic particles can be captured successfully at physiological flow rates even to the extent that emboli are formed. Mathematical modelling of the magnetic capture of magnetic nanoparticles from flows has also been undertaken (Voltairas et al. 2002; Furlani and Furlani 2007; Li et al. 2007; Shapiro et al. 2007; Hallmark et al. 2008; Le Drogoff et al. 2008). In the most recent attempt to model this capture, it was discovered that trapped nanoparticle layers formed from the capture of small 320 nm nanoparticle agglomerates were more stable to flow erosion than layers of larger 580 nm nanoparticle agglomerate (Hallmark et al. 2008). This modelling work also predicted that embolisms of captured particles were more likely to form in larger microcapillaries (800  $\mu\text{m}$  in diameter) at slower volumetric flow rates. This modelling work was based on experimental observations of nanoparticle capture in a constant flow rate regime through a single microcapillary (Darton et al. 2008b).

In order to further improve this *in vitro* model, an array of seven microcapillaries embedded within a plastic microcapillary film (MCF; Hallmark et al. 2005a, b) was used to allow a closer approximation of a constant pressure flow regime, which better mimics microcapillary networks *in vivo* (Darton et al. 2009). The presented results demonstrated that the magnetic field at the location of nanoparticle capture can vary significantly and that this variation is related to the net flow rate through the microcapillary array. A hypothesis is presented which gives a possible explanation for the underlying physics of capture and introduces the possibility of optimising field shape and strength for nanoparticle capture.

## Methods

### Superparamagnetic nanoparticle synthesis and characterisation

Superparamagnetic nanoparticles were prepared by precipitation from an iron (II) and iron (III) chloride solution on addition of ammonia solution following a published method of Ma et al. (2006). In transmission electron microscopy (TEM) (Philips CM100, 100 kV), the core particles synthesised can be seen to have diameters of around 10 nm (Fig. 1). These

core particles were found to aggregate into agglomerates with a mean hydrodynamic diameter of  $500 \pm 6$  nm as measured by Zeta-sizing (ZetaPALS sizer, Brookhaven, Holtsville, New York). These particle sizes were considered suitable for this study because they were large enough to enable in flow capture with a 0.5 T NdFeB magnet, but are still relatively small to potentially improve tissue penetration at target site. In order to reduce possible surface coat interactions or unevenness as well as prevent a reduction in magnetic saturation, no encapsulation of particles was used. Magnetic characterisation of the nanoparticles was performed in a Vibrating Sample Magnetometer (VSM) at 300 K in a sweep of magnetic fields from 1.5 to  $-1.5$  T and back to 1.5 T to check for the absence of hysteresis. The particles were seen to have a typical superparamagnetic nanoparticle magnetic response (Fig. 2). The Langevin equation (Connolly et al. 2005) for superparamagnetic particles was seen to fit the VSM data (Fig. 2) to give the magnetic moment per particle as  $141 \mu_B$ . The saturation magnetization was found to be  $66.0 \text{ Am}^2 \text{ kg}^{-1}$ , which is comparatively a high value for magnetite nanoparticles (Gupta and Gupta 2005). The nanoparticles were also found to have a magnetite lattice structure as determined by X-ray diffraction (Philips PW1820) and high-resolution TEM (Jeol 4000EX TEM, 400 kV acceleration voltage).

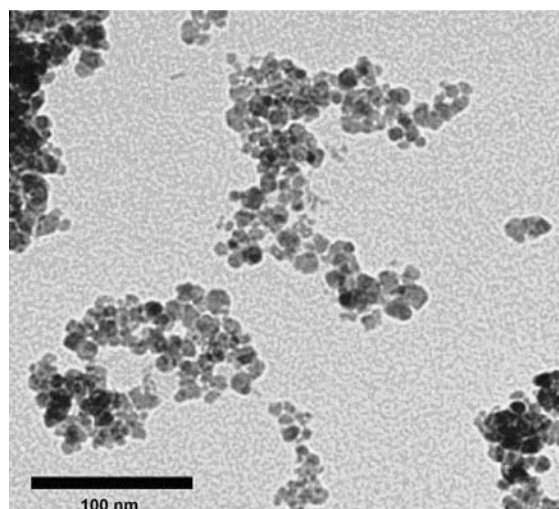
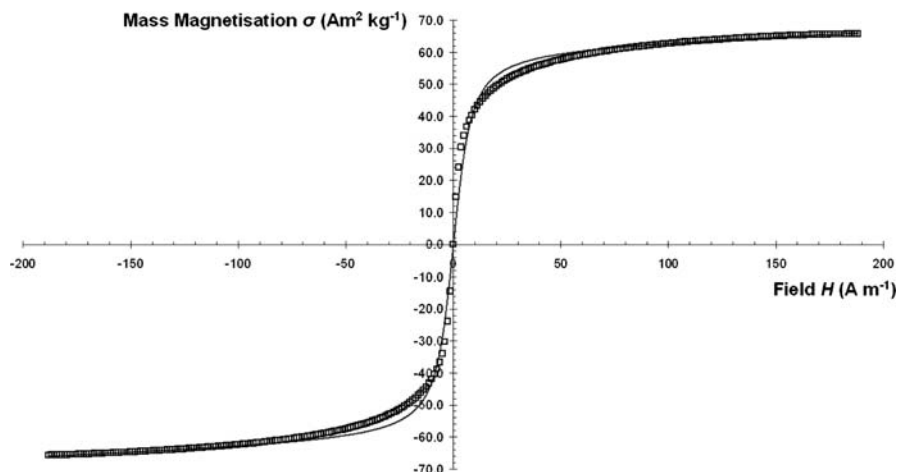


**Fig. 1** Transmission electron micrograph of magnetite superparamagnetic nanoparticles. The nanoparticles of diameter around 10 nm can be seen to form larger agglomerates (the black scale bar is 100 nm)

**Fig. 2** Vibrating Sample Magnetometer data showing typical magnetic response expected from magnetite nanoparticles from the absence of hysteresis and magnetic saturation of  $66.0 \text{ Am}^2 \text{ kg}^{-1}$ . The line shows that the data fits the Langevin fit to give a magnetic moment of  $141 \mu_B$



### Magnetic field mapping

A 0.5 T NdFeB permanent magnet of dimensions  $50 \times 50 \times 25 \text{ mm}$  (e-magnets, Sheffield, UK) was placed half-way along the MCF such that a spatially varying magnetic field existed across the capillary array. The magnetic field around the magnet was characterised using a Hall probe, with one corner of the magnet designated as the origin, as illustrated in Figs. 3 and 4. The magnetic field was then measured in the  $x$ ,  $y$  and  $z$  planes at each node in one quarter of the grid shown in Fig. 3 by rotating the Hall probe such that the flat tip of the probe was in the plane of measurement. Visualisation of the magnetic field using iron filings had demonstrated that the magnetic field was essentially symmetric around the centre of the magnet.

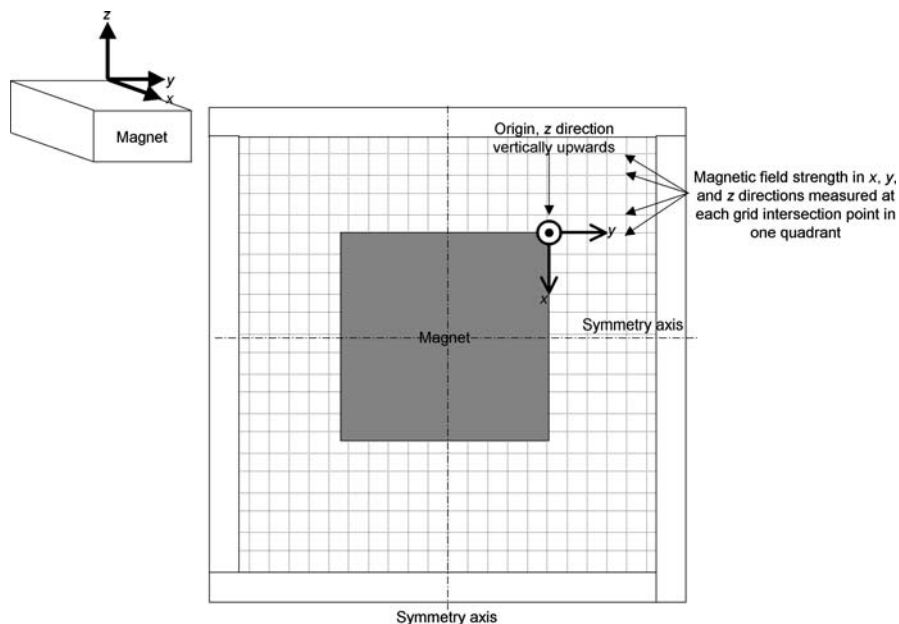
### Flow rig arrangement and experimental protocol

Figure 4 shows the flow rig that was used to observe the particle capture from flows within an array of seven microcapillaries. The microcapillary array consisted of a novel, plastic extrudate roughly  $400 \times 8.5 \times 0.54 \text{ mm}$  in dimensions, which is termed a microcapillary film (MCF) (Hallmark et al. 2005a, b). MCFs contain parallel arrays of microcapillaries embedded within a ribbon-like plastic film, as illustrated by the cross-sectional photograph (inset into Fig. 4); the capillaries in the MCF that were used for this study had a mean hydraulic diameter of  $210 \mu\text{m}$ . The MCF was fabricated from a linear low-density polyethylene (LLDPE) and was

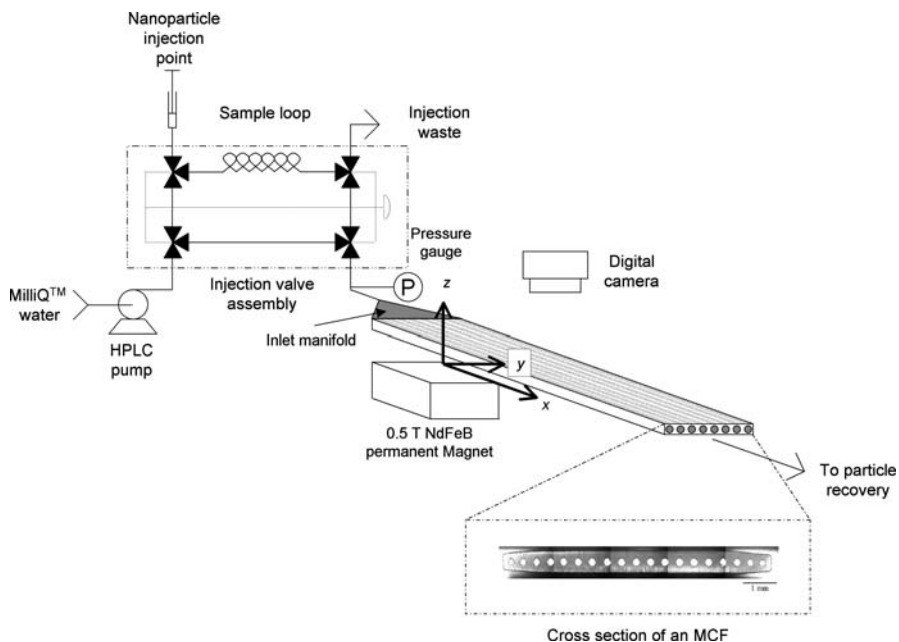
optically transparent and flexible. The central seven capillaries within this MCF were connected (the remainder being heat-sealed closed) to an HPLC pump (Kontron 422, Kontron Instruments, Milan, Italy), and the flow rate could be accurately controlled. Superparamagnetic nanoparticles were introduced into the bulk flow, before the MCF, using an HPLC injection valve (VICI Valco, Houston, TX). The flow then entered the MCF and split between the seven capillaries. If one, or more, capillary or capillaries presented an increased resistance to flow compared to the remainder (for example, by partial blockage with nanoparticles), then the flow was able to redistribute across the capillary array. In this way, the pressure drop across the capillary array as a whole could remain relatively constant. The location of the black-coloured nanoparticles within the MCF was imaged with a digital camera (Canon IXUS 800 IS).

The experimental procedure consisted of initially setting the flow rate to  $0.2 \text{ mL min}^{-1}$  and releasing a slug of nanoparticles, approximately  $2 \text{ mL}$  in volume with a concentration of  $7 \text{ mg mL}^{-1}$ , into the flow using the injection valve. Subsequent nanoparticle capture by the magnet was imaged at regular time intervals until a steady-state layer of captured nanoparticles formed. Steady-state was considered to occur when the location and appearance of the captured nanoparticle layer remained unaltered for a period of 10 min. The MCF was then flushed with MilliQ water at approximately  $10 \text{ mL min}^{-1}$  to remove the captured nanoparticles. The experiment was then repeated at flow rate increments of  $0.2 \text{ mL min}^{-1}$  up to a flow rate of  $2.0 \text{ mL min}^{-1}$ .

**Fig. 3** Schematic diagram showing a representation of the grid that was used to characterise the magnetic field



**Fig. 4** Schematic diagram of the flow rig



## Results and discussion

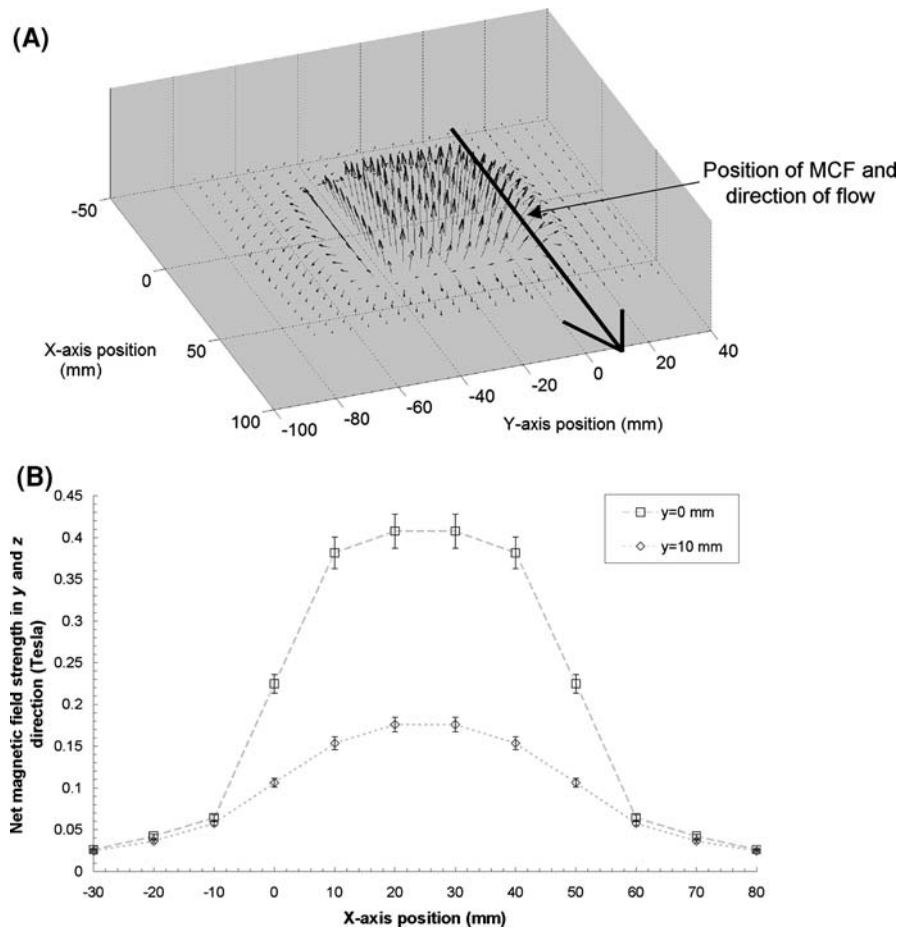
### Magnetic field characterisation

The plots in Fig. 5 show the form of the magnetic field around the magnet. The plot in Fig. 5a shows vectors representing the direction and strength of the magnetic field across a plane at  $z = 0$ . The north and south poles of the magnet are on the upper and the

lower faces of the magnet and the MCF is positioned along an edge at a constant  $y$  location, i.e. at a constant distance from the magnet, with the flow within the capillaries running in the  $x$  direction. This is shown by the large arrow in this figure, with the arrow pointing towards the direction of flow.

The plot in Fig. 5b shows the variation in magnetic field in the flow direction at two different positions in the  $y$  direction, at  $y = 0$  mm, along the edge of the

**Fig. 5 a** Vector plot of the magnetic field as a function of  $x$  and  $y$  locations at a fixed plane in the  $z$  direction. The *large arrow* shows the approximate spatial location of the MCF with respect to the magnet that was used in the flow rig. **b** Plot of the net magnetic field in the  $x$  and  $y$  directions as a function of  $x$ -axis position for two different  $y$  locations



magnet, and at  $y = 10$  mm, 10 mm away from the edge of the magnet. The position of the MCF with respect to the magnet within the flow loop fell within these two  $y$  locations and hence this figure provides quantitative information relating to the strength of the magnetic field as a function of position within the flow direction. Field strengths at points between  $y = 0$  and 10 mm, relating to the field strength in individual capillaries, were found by polynomial interpolation of the field in the  $y$  direction.

**Magnetic capture results**

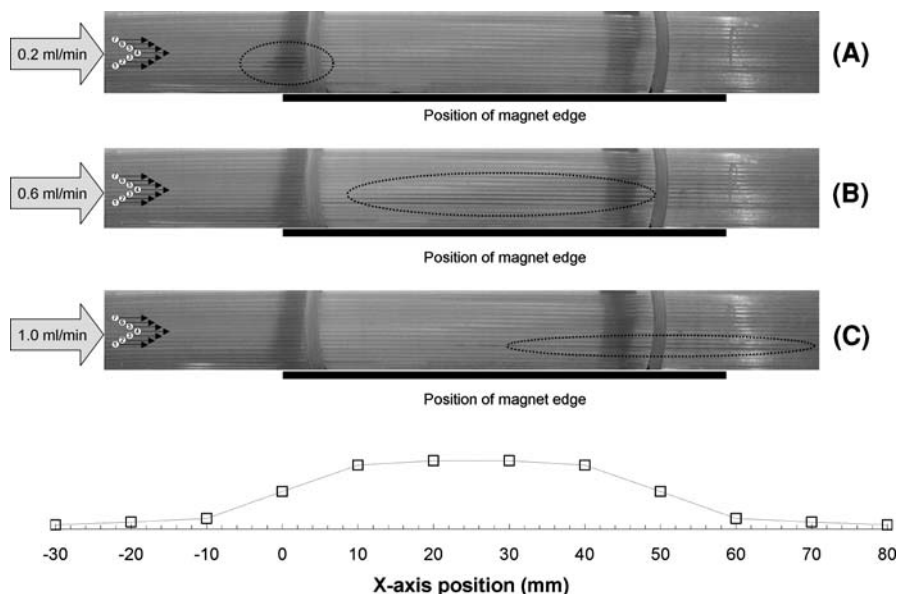
The sequence of images in Fig. 6 show that it is possible to capture superparamagnetic nanoparticles flowing within an array of microcapillaries, and that the position of the captured slug varies substantially with flow rate. In each of these images, the

nanoparticles flow in from the left through seven microcapillaries (in the direction of the arrows) and are captured at a location circled by the dotted ellipse. Also, in this figure, a plot shows the shape of the magnetic field in the flow direction indicating where the maxima and minima of the magnetic field lie; this plot has been scaled such that it can be compared directly to the photographs and to the position of the captured slug of nanoparticles. It should be noted that the absolute magnitude of the field will diminish with distance away from the magnet, as illustrated by the plot in Fig. 5b, but the overall form will remain the same.

Several interesting observations can be made from these images. First, it can be seen that nanoparticles can be successfully captured in more than one capillary, but the length of the captured nanoparticle layer diminishes with distance away from the magnet.



**Fig. 6** Photographs illustrating the position of nanoparticle capture for volumetric flow rates of **a**  $0.2 \text{ mL min}^{-1}$ , **b**  $0.6 \text{ mL min}^{-1}$  and **c**  $1.0 \text{ mL min}^{-1}$ . The location of capture has been highlighted with the *dotted line*, and the magnet was situated at the base of the MCF in each picture. The graph at the base of the image illustrates the form of the magnetic field as a function of position in the  $x$  direction and has been scaled to match the photographs



It can also be seen that as the flow rate increases, the position of the captured nanoparticle layer moves progressively downstream and that the overall length of the captured layer increases. It is also apparent that capture occurs in increasingly fewer capillaries and the higher the flow rate becomes, with the capillaries within which capture is observed, being those closest to the magnet. It is also interesting to note that as the location of the captured nanoparticles moves further downstream with increasing flow rate, the strength of the magnetic field at the furthest downstream point of the captured layer becomes significantly lower. The strength of the magnetic field at the furthest upstream location of the captured layer, however, displays the reverse trend in that it rises.

The plots in Fig. 7 show the latter two of these trends quantitatively. Figure 7a shows how the magnetic field strength at the most upstream point of the captured nanoparticle layer increases and then plateaus as a function of flow rate for the capillary nearest to and the capillary furthest from the magnet. The plot in Fig. 7b shows how the magnetic field at the most downstream point of the captured layer at first increases significantly as a function of flow rate, but then rapidly decreases to an essentially constant value at the higher flow rates and that this value is the lowest magnetic field strength observed for all flow rates. These two trends are reflected across the entire

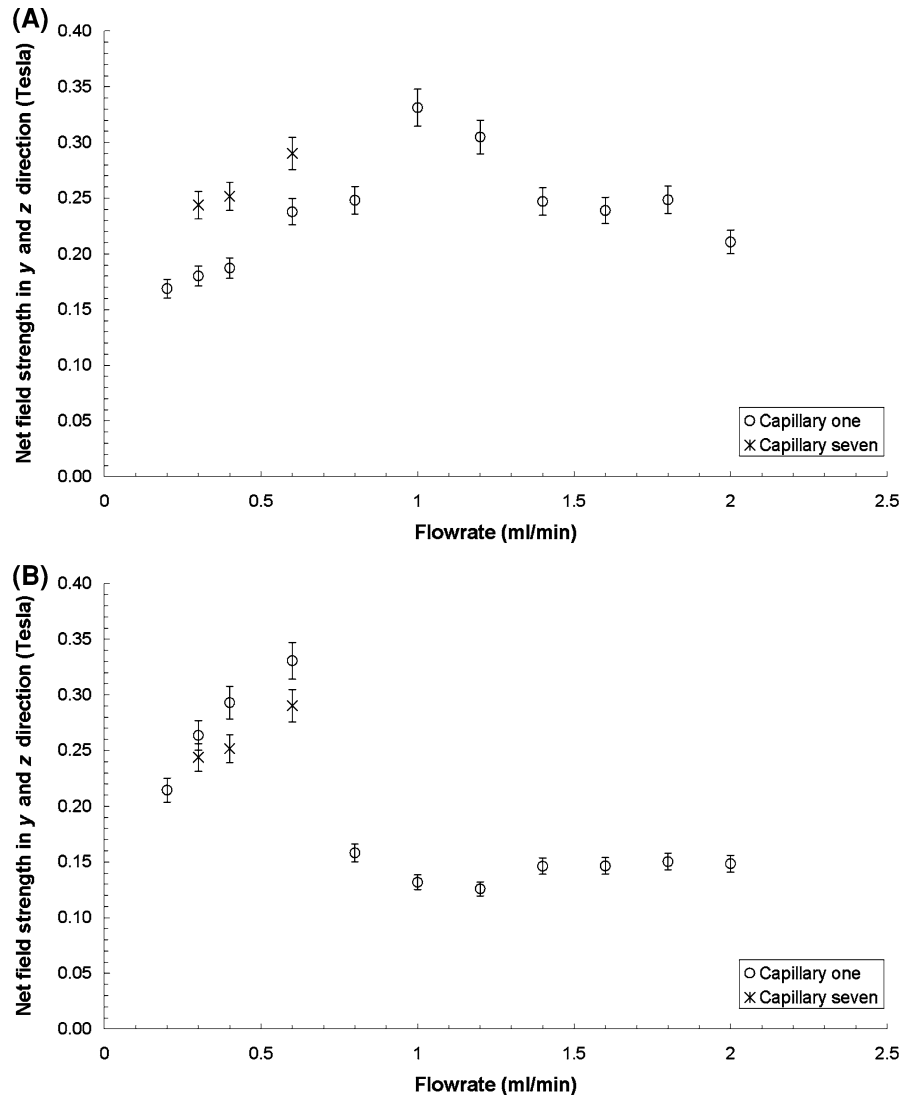
capillary array, the key difference being that nanoparticle capture is only possible at lower flow rates in capillaries furthest from the magnet.

## Discussion

The experimental data indicate the complex dynamics of superparamagnetic nanoparticles when subjected to a combination of fluid flow and a magnetic field. The relevant physical phenomena for movement of particles under the influence of magnetic fields have been previously described (Clime et al. 2008). Consider the balance between the two competing effects; the force on the particles due to the magnetic field acts to steer, capture and immobilise the magnetic nanoparticles, whilst that due to the flow acts to convey particles and to erode any layer of nanoparticles that may have been captured. Capture depends on whether the magnetic field is strong enough to steer the nanoparticles to a capillary wall and, if so, whether the magnetic field at that point is strong enough to overcome erosion.

Furlani and Furlani (2007) show calculations relating to the trajectories of individual nanoparticles that are subjected to both a laminar flow field and a magnetic field. Whether a nanoparticle arrives at a capillary wall or whether it is conveyed by the flow away from the magnet is governed by its trajectory

**Fig. 7** Plots showing the absolute magnetic field strength at **a** the most upstream point and **b** the most downstream point of the ‘slug’ of captured nanoparticles as a function of flow rate for the capillary nearest to the magnet (capillary 1) and the capillary furthest from the magnet (capillary 7)



through the flow in the capillary. The trajectory of the nanoparticle is determined by the relative magnitudes of the radial and axial velocities of the nanoparticle. The axial velocity of the nanoparticle can be approximated to be the same as the fluid velocity at the radial location of the nanoparticle,  $u_z(r)$ , where

$$u_z(r) = 2\langle u \rangle \left( 1 - \frac{r^2}{R^2} \right). \tag{1}$$

Here,  $r$  is the radial position of the nanoparticle within the capillary,  $R$  is the capillary radius,  $\langle u \rangle$  is the average axial fluid velocity and  $u_z(r)$  is the axial velocity at a given radial position. The radial velocity

of the nanoparticle at a specific axial location,  $u_r$ , is proportional to the gradient of the square of the absolute magnetic field strength,  $|\mathbf{H}|$ , i.e.

$$u_r \propto \frac{\partial}{\partial y} (|\mathbf{H}|^2). \tag{2}$$

Previous experimental and modelling have shown that if nanoparticles do arrive at a capillary wall, capture only occurs when magnetic forces dominate the hydraulic forces (Darton et al. 2008b; Hallmark et al. 2008). Incipient capture can be assumed to occur at the spatial location where hydraulic forces and magnetic forces are equal. As the magnetic force on a nanoparticle,  $F_{m,y}$ , is also proportional to the

gradient of the square of the absolute magnetic field strength, i.e.

$$F_{m,y} \propto \frac{\partial}{\partial y} (|\mathbf{H}|^2), \quad (3)$$

and that the hydraulic force on a nanoparticle is directly proportional to the axial velocity or volumetric flow rate,  $Q$ , i.e.

$$\begin{aligned} F_h &\propto u_z \\ F_h &\propto Q. \end{aligned} \quad (4)$$

The first set of experimental observations relate to the position of the captured nanoparticle layer, both as a function of increasing flow rate and as a distance away from the magnet. These observations are characterised by the increasing dominance of hydraulic forces compared to the magnetic forces within the capillary array. If nanoparticles arrive at a capillary wall, and if at that location, the force on the nanoparticles due to the magnetic field exceeds the force due to hydraulic shear, then the nanoparticles will be captured. If the force due to hydraulic shear, however, exceeds the force due to the magnetic field, then the nanoparticles will not be captured but rather they will move with the flow along the capillary. As the flow in a capillary increases, the hydraulic forces also increased as a result of Eq. (4).

Hydraulic forces then become increasingly dominant at higher flow rates and fewer particles are captured. In addition, higher fluid velocities result in nanoparticle trajectories that are less likely to bring them in contact with a capillary wall, even in the region where magnetic forces are dominant. In a similar manner, for a constant fluid velocity, magnetic forces diminish with increasing distance from the magnet. In the plots given in Fig. 5a and b, the absolute magnetic field strength decreases nonlinearly with increasing perpendicular distance from the magnet. Hence,  $\frac{\partial}{\partial y} (|\mathbf{H}|^2)$  and the magnetic forces also decrease and the likelihood of nanoparticle capture is diminished.

Figure 8a shows two sets of nanoparticle trajectories representing nanoparticles travelling at a constant radial velocity across a parabolic flow profile. The assertion of constant radial velocity means that  $\frac{\partial}{\partial y} (|\mathbf{H}|^2)$  is constant. From Fig. 5b, it can be written that

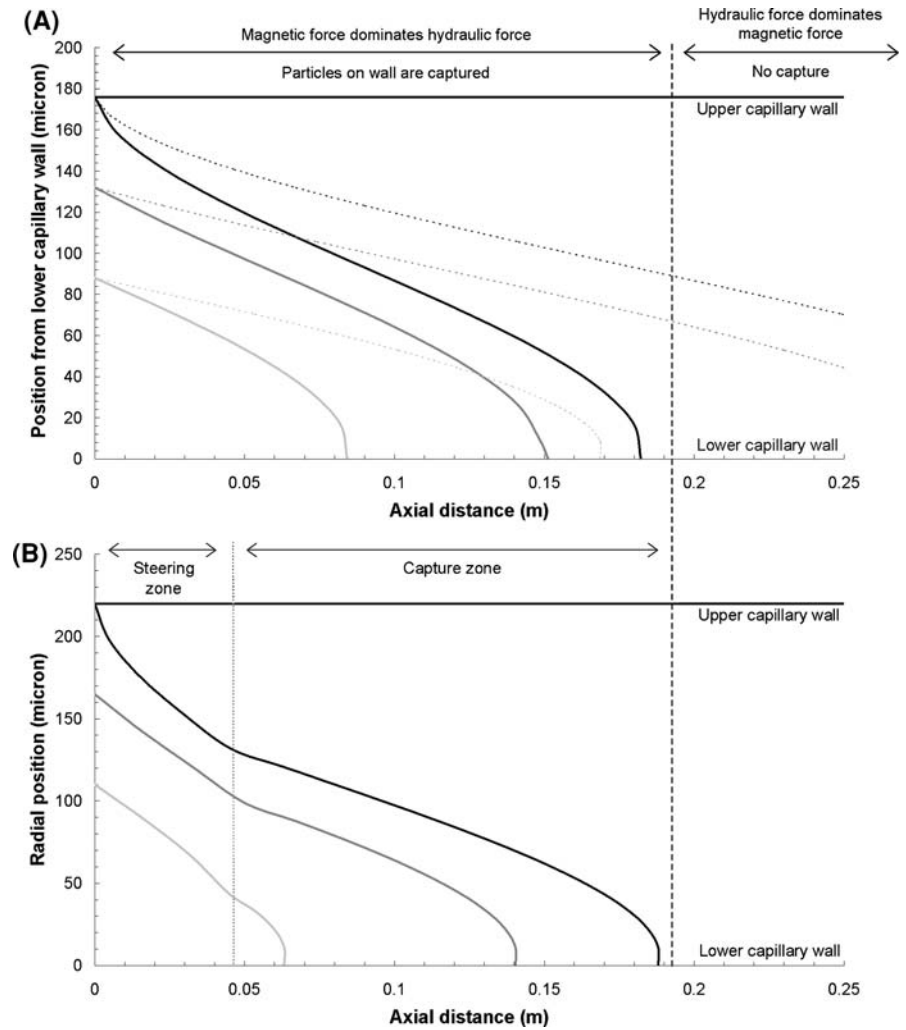
$$\frac{\partial}{\partial y} (|\mathbf{H}|^2) \approx \frac{|\mathbf{H}|_{y=0}^2 - |\mathbf{H}|_{y=10}^2}{\Delta y}. \quad (5)$$

The assertion of constant radial velocity is reasonable between axial locations of roughly 15 and 35 mm since, at these locations, the experimentally measured magnetic field strength (curves) shown in Fig. 5 is at maximum and the numerator of Eq. (5) will be approximately constant. The axial velocity of the nanoparticles represented by the bold trajectories is smaller than that of the nanoparticles represented by the feint lines; thus, the bold trajectories correspond to lower volumetric flow rates than the feint trajectories. Also marked in Fig. 8a is a region where the force on the nanoparticles due to the magnetic field exceeds that due to hydraulic forces. Again, referring to Fig. 5b, it can be seen that the absolute magnetic field strength decays sharply at axial locations  $>40$  mm. There will also be a corresponding decrease in the gradient of  $|\mathbf{H}|^2$  and therefore, according to Eq. (3), the magnetic force on the nanoparticle. It is therefore reasonable to assume that, at some axial location  $>40$  mm, the magnetic force will weaken significantly and that hydraulic forces will become dominant. It can be seen from Fig. 8a that the trajectories of the nanoparticles represented by the bold lines all reach the capillary wall and are able to be captured, whereas only one of the trajectories represented by the feint lines reach the wall in the ‘capture zone’, the remainder being conveyed away from the influence of the magnetic field before they reach the wall.

A second set of experimental observations, relating to the change in magnetic field strengths at the furthest upstream and downstream points of the captured nanoparticle layer as a function of flow rate, can also be explained by the diagram shown in Fig. 8a, along with the plot shown in Fig. 5b. To simplify the argument, it is assumed the boundary between the zone where particles are captured and where particles are not captured, represented by the dashed vertical line running through both Fig. 8a and b, is in the region of decreasing field strength in the plot shown in Fig. 5b, say, for example, at an axial location  $>40$  mm. The black line that originates from the upper wall of the capillary represents the trajectory of a nanoparticle starting at that wall, furthest from the magnet; this trajectory finishes at



**Fig. 8** Qualitative plots showing the trajectory of particles released at points in a laminar flow for **a** particles having a uniform radial velocity resulting from ‘strong’ (*bold lines*) and ‘weak’ (*feint lines*) magnetic fields and **b** particles having non-uniform radial velocities, where the radial velocity in the steering zone is double that of the capture zone. This schematically represents trajectories for particles subject to an initially strong, but decaying magnetic field



the lower wall within the region where nanoparticles are captured. It can therefore be concluded that if this nanoparticle reaches the lower wall, then all the nanoparticles are captured (total capture) and that the point of intersection between the black trajectory and the wall represents the furthest downstream position of the captured nanoparticle layer. It can be seen that the field strength at the furthest downstream position of the nanoparticle layer for total capture is greater than the minimum field strength required to capture nanoparticles; hence, the field measured at the end of the captured layer will be higher than the minimum value required to immobilise nanoparticles.

For the feint dotted trajectories, representing increased axial flow the dotted black trajectory that

originates from the upper capillary wall does not reach the lower wall. The light grey trajectory, originating from the centre of the flow, does however reach the lower wall in the region where nanoparticles will be captured. The physical interpretation of this is that only some of the nanoparticles are captured; this is termed partial capture. The layer of nanoparticles under the regime of partial capture, though, will only extend downstream so long as magnetic forces are dominant; the magnetic field strength at the furthest downstream point of the captured layer will hence be the minimum field strength required to capture nanoparticles for a given set of hydraulic and magnetic conditions.

The two key results of this hypothesis are that magnetic field strengths measured at the end of the

captured nanoparticle layer will be (a) higher than the minimum required field for capture under the regime of total capture and (b) constant at the minimum level required for capture under the regime of partial capture. These findings are consistent with the experimental data.

This hypothesis also provides fundamental logic for the design of magnetic field shape and strength for effective nanoparticle capture. The diagram shown in Fig. 8b shows three nanoparticle trajectories where the radial velocity of the nanoparticles changes with respect to axial position; the radial velocity between axial positions of 0 and 45 mm is double that for the remainder of the axial locations. This can be likened to tailoring the shape of the magnetic field along the length of the capillary, remembering that the magnetic force is related to the absolute magnetic field strength by Eq. (3). It can be seen firstly that total capture is achieved, but also that all the capture occurs in the region where the radial velocity of the particles is lower, representing a lower magnetic field strength. The short region where the radial velocity is highest, representing a high magnetic field, results in steering the nanoparticles sharply away from their original location across the bulk of the flow, and closer to the lower wall; this region is termed the ‘steering zone’. Capture takes place in the longer region where the radial velocity is lower, representing a weaker magnetic field, but where the bulk of the non-captured particles have been moved close to the lower wall by the steering zone; this region is termed the ‘capture zone’.

This result could have an important implication for targeting nanoparticles *in vivo* where it may not always be practical to use one strong magnet to capture nanoparticles. It may be that a magnet providing a ‘steering’ zone could be placed externally near an arteriole and then a series of significantly smaller magnets, providing the ‘capture zone’ could then be implanted where required. It may be unlikely that these smaller magnets alone would be able to cause enough partial capture for a therapeutic response, but in combination with a larger magnet providing a ‘steering zone’ prior to capture, significant partial capture or even total capture may be possible. This theory does, however, need significant future research to assess its viability and to optimise magnetic field architecture and strength.

## Conclusion

This paper has presented data on the capture of superparamagnetic nanoparticles from a laminar flow within a capillary array. The key finding is that it is possible to immobilise superparamagnetic nanoparticles over a wide range of flow rates and spatial locations with respect to the magnet that provides the field for capture. Consequently, the magnetic field strength measured at the point of nanoparticle capture, and hence the field strength required to immobilise nanoparticles, can vary greatly. A hypothesis has been suggested to explain these findings, which suggests that the measured variation in magnetic field strength at the most downstream point of capture relates to two regimes of nanoparticle capture, total capture and partial capture. Furthermore, this hypothesis suggests that the strategic use of different strength magnets in different spatial locations, providing ‘steering zones’ and ‘capture zones’, may enable the magnetic field shapes and strengths to be optimised to improve the effectiveness of nanoparticle capture *in vivo*.

In future, rigorous mathematical modelling of the hypothesis outlined in this study will provide further insight into its validity whilst also giving a quantitative prediction of the strengths and shapes of the magnetic fields required for capture. This will be reinforced by adapting the experimental techniques outlined in this study to investigate the effect of shaped magnetic fields on the dynamics of nanoparticle capture. If successful, the evidence from these studies could provide enough data for future *in vivo* research.

**Acknowledgements** The authors would like to acknowledge both the BBSRC and the EPSRC for funding, Alexander Barcza for help with the VSM and X-ray diffraction analysis and Dr. Caterina Ducati for help with the high-resolution TEM analysis (Department of Material Science and Metallurgy, Cambridge University).

## References

- Clime L, Le Drogoff B, Zhao S et al (2008) Magnetic nanocarriers: from material design to magnetic manipulation. *Int J Nanotechnol* 5(9–12):1268–1305. doi:10.1504/IJNT.2008.019839
- Connolly J, St Pierre TG, Dobson J (2005) Experimental evaluation of the magnetic properties of commercially

- available magnetic microspheres. *Biomed Mater Eng* 15(6):421–431
- Darton NJ, Hallmark B, Han X et al (2008a) The in-flow capture of superparamagnetic nanoparticles for targeting of gene therapeutics. In: American institute of physics conference proceedings, vol 1025, pp 20–27
- Darton NJ, Hallmark B, Han X et al (2008b) The in-flow capture of superparamagnetic nanoparticles for targeting therapeutics. *Nanomedicine NBM* 4(1):19–29
- Darton NJ, Hallmark B, James T et al (2009) Magnetic capture of superparamagnetic nanoparticles in a constant pressure microcapillary flow. *J Magn Magn Mater*. doi:[10.1016/j.jmmm.2009.02.088](https://doi.org/10.1016/j.jmmm.2009.02.088)
- Furlani EJ, Furlani EP (2007) A model for predicting magnetic targeting of multifunctional particles in the microvasculature. *J Magn Magn Mater* 312(1):187–193. doi:[10.1016/j.jmmm.2006.09.026](https://doi.org/10.1016/j.jmmm.2006.09.026)
- Gupta AK, Gupta M (2005) Synthesis and surface engineering of iron oxide nanoparticles for biomedical applications. *Biomaterials* 26(18):3995–4021. doi:[10.1016/j.biomaterials.2004.10.012](https://doi.org/10.1016/j.biomaterials.2004.10.012)
- Hallmark B, Gadala-Maria F, Mackley MR (2005a) The melt processing of polymer microcapillary film (MCF). *J Non Newton Fluid* 128(2–3):83–98. doi:[10.1016/j.jnnfm.2005.03.013](https://doi.org/10.1016/j.jnnfm.2005.03.013)
- Hallmark B, Mackley MR, Gadala-Maria F (2005b) Hollow microcapillary arrays in thin plastic films. *Adv Eng Mater* 7:545–547. doi:[10.1002/adem.200400154](https://doi.org/10.1002/adem.200400154)
- Hallmark B, Darton NJ, Han X et al (2008) Observation and modelling of capillary flow occlusion resulting from the capture of superparamagnetic nanoparticles in a magnetic field. *Chem Eng Sci* 63(15):3960–3965. doi:[10.1016/j.ces.2008.04.057](https://doi.org/10.1016/j.ces.2008.04.057)
- Kikura H, Matsushita J, Kakuta N et al (2007) Cluster formation of ferromagnetic nano-particles in micro-capillary flow. *J Mater Process Technol* 181(1–3):93–98. doi:[10.1016/j.jmatprotec.2006.03.013](https://doi.org/10.1016/j.jmatprotec.2006.03.013)
- Le Drogoff B, Clime L, Veres T (2008) The influence of magnetic carrier size on the performance of microfluidic integrated micro-electromagnetic traps. *Microfluid Nano-fluidics* 5(3):373–381. doi:[10.1007/s10404-007-0249-1](https://doi.org/10.1007/s10404-007-0249-1)
- Li XL, Yao KL, Liu HR et al (2007) The investigation of capture behaviors of different shape magnetic sources in the high-gradient magnetic field. *J Magn Magn Mater* 311(2):481–488. doi:[10.1016/j.jmmm.2006.07.040](https://doi.org/10.1016/j.jmmm.2006.07.040)
- Liu J, Flores GA, Sheng RS (2001) In-vitro investigation of blood embolization in cancer treatment using magneto-rheological fluids. *J Magn Magn Mater* 225(1–2):209–217. doi:[10.1016/S0304-8853\(00\)01260-9](https://doi.org/10.1016/S0304-8853(00)01260-9)
- Lubbe AS, Bergemann C, Riess H et al (1996) Clinical experiences with magnetic drug targeting: a phase I study with 4'-epidoxorubicin in 14 patients with advanced solid tumors. *Cancer Res* 56(20):4686–4693
- Lubbe AS, Bergemann C, Brock J et al (1999) Physiological aspects in magnetic drug-targeting. *J Magn Magn Mater* 194(1–3):149–155. doi:[10.1016/S0304-8853\(98\)00574-5](https://doi.org/10.1016/S0304-8853(98)00574-5)
- Ma ZY, Guan YP, Liu HZ (2006) Superparamagnetic silica nanoparticles with immobilized metal affinity ligands for protein adsorption. *J Magn Magn Mater* 301(2):469–477. doi:[10.1016/j.jmmm.2005.07.027](https://doi.org/10.1016/j.jmmm.2005.07.027)
- Sako M, Hirota S, Ohtsuki S (1986) Clinical evaluation of ferromagnetic microembolization for the treatment of hepatocellular carcinoma. *Ann Radiol (Paris)* 29(2):200–204
- Shapiro B, Probst R, Potts HE et al (2007) Control to concentrate drug-coated magnetic particles to deep-tissue tumors for targeted cancer chemotherapy. In: Proceedings of the 46th IEEE conference on decision and control, 1–14 Dec 2007, pp 5126–5131
- Sheng R, Flores GA, Liu J (1999) In vitro investigation of a novel cancer therapeutic method using embolizing properties of magnetorheological fluids. *J Magn Magn Mater* 194(1–3):167–175. doi:[10.1016/S0304-8853\(98\)00565-4](https://doi.org/10.1016/S0304-8853(98)00565-4)
- Udrea LE, Strachan NJ, Badescu V et al (2006) An in vitro study of magnetic particle targeting in small blood vessels. *Phys Med Biol* 51(19):4869–4881. doi:[10.1088/0031-9155/51/19/010](https://doi.org/10.1088/0031-9155/51/19/010)
- Voltairas PA, Fotiadis DI, Michalis LK (2002) Hydrodynamics of magnetic drug targeting. *J Biomech* 35(6):813–821. doi:[10.1016/S0021-9290\(02\)00034-9](https://doi.org/10.1016/S0021-9290(02)00034-9)
- Wilson MW, Kerlan RK, Fidelman NA et al (2004) Hepatocellular carcinoma: regional therapy with a magnetic targeted carrier bound to doxorubicin in a dual MR imaging/conventional angiography suite—initial experience with four patients. *Radiology* 230(1):287–293. doi:[10.1148/radiol.2301021493](https://doi.org/10.1148/radiol.2301021493)